Japanese Journal of Applied Physics

REGULAR PAPERS

A simple way to higher speed atomic force microscopy by retrofitting with a novel high-speed flexure-guided scanner

To cite this article: Bernard Ouma Alunda *et al* 2018 *Jpn. J. Appl. Phys.* **57** 06HJ02

Japanese Journal of Applied Physics **57**, 06HJ02 (2018)
https://doi.org/10.7567/JJAP.57.06HJ02

REGULAR PAPER

A simple way to higher speed atomic force microscopy by retrofitting with a novel high-speed flexure-guided scanner

Bernard Ouma Alunda[1], Yong Joong Lee[1*], and Soyeun Park[2*]

[1]*School of Mechanical Engineering, Kyungpook National University, Daegu 41566, Republic of Korea*
[2]*College of Pharmacy, Keimyung University, Daegu 42601, Republic of Korea*

*E-mail: yjlee76@knu.ac.kr; sypark20@kmu.ac.kr

Received December 2, 2017; revised January 23, 2018; accepted February 22, 2018; published online May 8, 2018

A typical line-scan rate for a commercial atomic force microscope (AFM) is about 1 Hz. At such a rate, more than four minutes of scanning time is required to obtain an image of 256 × 256 pixels. Despite control electronics of most commercial AFMs permit faster scan rates, default piezoelectric *X*–*Y* scanners limit the overall speed of the system. This is a direct consequence of manufacturers choosing a large scan range over the maximum operating speed for a *X*–*Y* scanner. Although some AFM manufacturers offer reduced-scan area scanners as an option, the speed improvement is not significant because such scanners do not have large enough reduction in the scan range and are mainly targeted to reducing the overall cost of the AFM systems. In this article, we present a simple parallel-kinematic substitute scanner for a commercial atomic force microscope to afford a higher scanning speed with no other hardware or software upgrade to the original system. Although the scan area reduction is unavoidable, our modified commercial XE-70 AFM from Park Systems has achieved a line scan rate of over 50 Hz, more than 10 times faster than the original, unmodified system. Our flexure-guided *X*–*Y* scanner can be a simple drop-in replacement option for enhancing the speed of various aging atomic force microscopes.

1. Introduction

Atomic force microscopy has been one of the most versatile microscopy methods for research in the field of nanotechnology compared to scanning tunneling microscopy (STM), scanning electron microscopy (SEM), and transmission electron microscopy (TEM) because of several advantages. Atomic force microscopy (AFM) permits scanning in vacuum, gaseous or even in liquid environments. Also, atomic force microscopy has little or no restrictions on sample preparations and experimental environments. AFM can be used for imaging,[1–9] force spectroscopy[10–13] and nano-fabrication.[14,15] In force spectroscopy, an AFM is used for measuring forces between a probe and a sample down to the femto-Newton (fN) range[16] whereas for imaging, the interaction forces between the cantilever tip and the sample is used to construct three-dimensional images of a sample topography with sub-nanometer lateral and sub-angstrom vertical resolutions.[17,18] Nano-fabrication on the other hand involves making structures with dimensions in the nanometer range (≤100 nm) by using micro- and nano-manipulators,[19–21] force lithography,[22] nano-indentation,[23–26] dip-pen lithography,[27] and nano-oxidation.[28–31] Although the versatility of AFMs has put the tool on the forefront in nanoscience and nano-engineering research, further extensions in applications potentially require various improvements to be made on some aspects of the conventional AFM.

For operating an AFM at high speeds, three important aspects must be properly considered. First, the employed cantilever must have a high resonant frequency. Commercial AFM cantilevers with high bandwidths have already been developed and are available for purchase.[32,33] Second, a *Z*-scanner with a high bandwidth is required for maintaining the high speed feedback control. Third, a lateral *X*–*Y* scanner must also have a correspondingly high bandwidth for handling fast raster scanning. For most commercial AFMs, a single-image acquisition takes several to tens of minutes[32] since the line scan speed is typically around 1 Hz or lower. In addition, at slow speeds, the effects of creep associated with piezoelectric actuators is unavoidable, and this may cause a significant level of distortion in image quality. A previous report has shown that piezoelectric tube scanner-based commercial systems begin to oscillate along the fast scanning axis at a scan rate as low as 8 lines per second.[34] Also, using a common tube scanner has an added disadvantage of introducing cross-coupling in all three axes of the scanner, causing a serious variation in height commonly referred to as the bowing effect. This drawback has made it difficult to use most commercial AFMs in applications where speed is one of the primary factors and the scanner must be operated at a relatively high speed. Instead of developing all new hardware and software for high-speed atomic force microscopy, we have investigated the possibility of improving the scan speed of a commercial AFM with a minimal modification and found that most commercial AFMs' control electronics indeed allow higher scan rates than typically utilized. Therefore, the fundamentally limiting elements of typical AFMs for high speed operations are their slow *X*–*Y* scanners with a large scan range (usually 50–100 μm).

In this article, we present a simple upgrade path for increasing the operating speed of an aging commercial AFM by simply replacing the default scanner with a custom-made flexure-based parallel-kinematic piezoelectric scanner. The high stiffness of flexure-based scanners allows imaging at extended speeds on account of their high bandwidth and reduced mass of the moving central piece. Flexure mechanisms are very suitable for AFM scanners because of their ability to offer repeatable motions with high accuracy. This is brought about by their joint-less construction, monolithic and simple designs that eliminate complex mechanical assemblies. With the fabricated scanner incorporated into a commercial AFM, we demonstrate the increase in the scanning speed to above 50 Hz, more than 10 folds in improvement before *Z*-ringing[35] becomes a limiting factor for obtaining good topographic images.

2. Experimental procedure

First, the finite element analysis (FEA) using COMSOL Multiphysics has been carried out to optimize the parameters influencing the scan range and bandwidth of the scanner

during the initial design stage. After the model verifications, the designed scanner was fabricated from 6061 aluminum alloy because of its desirable characteristics such as low cost, ease of machining, and good electrical conductivity suitable for accurate electrical discharge machining (EDM) of the flexures.[36] EDM is the most preferred machining method for flexures as a consequence of its ability to create complex flexure shapes, a good finish that requires no additional machining, high tolerance and non-contact machining process that allows the fabrication of brittle and hard work pieces. Our scanner is monolithic and machined from a single piece of 6061 aluminum.

After the fabrication and assembly, the scanner was experimentally characterized to obtain its maximum scan range and bandwidth by using a capacitive sensor and a dynamic signal analyzer (DSA). The amount of cross-coupling and magnitude of intrinsic hysteresis in the scanner movements were also measured. Finally, the speed enhancement of the modified AFM system was demonstrated by scanning a Blu-ray disk at different scan speeds and analyzing the obtained topographic and error signal images.

3. Results and discussion

3.1 Design details of the proposed scanner

The proposed scanner is designed to operate with piezo stack actuators under preloaded condition. It is mechanically different from the so called the push–pull parallel kinematic-scanner proposed by Schitter et al.[37] Although the push–pull scanner has the advantage of maximizing the actuation force resulting in higher operating speed and increased range, it also has other drawbacks. The main drawback hindering its application toward upgrading a commercial AFM is the requirement for an increased number of power amplifiers. A push–pull type scanner needs two power amplifiers per axis. This means that for properly driving a two-dimensional push–pull scanner, a total of four power amplifiers are required. The fact that most commercial AFM control electronics have only one power amplifier per axis limits the application of the push–pull scanners without a significant level of modifications to the original system. For instance, a push–pull scanner can only be integrated to a typical AFM system by separately pulling low voltage piezo signals to the outside of the controller for further processing that includes complementary push–pull drive waveform generation and power amplification. This type of modification definitely adds more complexity to the overall system. Moreover, the push and pull voltage waveforms need to be precisely synchronized in order to minimize possible image distortions if no positioning feedback is implemented for the scanner operation. Our proposed scanner, however, does not require any additional power amplifier for its operation. Therefore, common AFM controllers should be able to drive the proposed scanner directly without any modification to their piezo drive electronics.

The overall size of the scanner is $136 \times 136\,\mathrm{mm}^2$ with a central moving platform having a circular bore of 36 mm in diameter. The central hole was an intentional implementation for allowing an approach to a sample by a microscope objective lens from below the scanner in future applications. This design approach, however, results in a reduced bandwidth of the scanner due to the increased size and mass of the moving part. If one does not require an optical access, the central platform can be designed to be smaller in size, thereby resulting in decreased mass and higher bandwidth. Each axis of the scanner has a combination of 1- and 2-mm-thick stiff flexures that are strategically positioned to minimize the level of deformation to the central moving platform with a circular bore when driven by piezo stacks. Also, the locations of piezo stacks and the thickness of flexures have been varied in simulations using finite element analysis to give the most desirable characteristics. More details of the simulation are given in the following section.

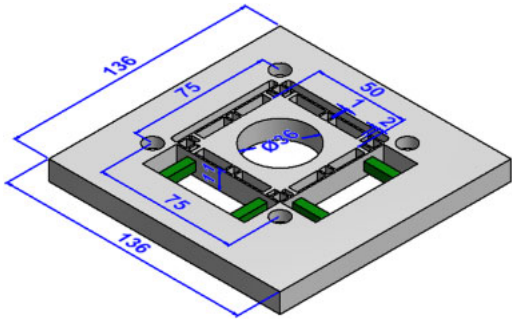

Fig. 1. (Color online) Dimensional details of the proposed high-speed scanner. All dimensions are in mm.

The out-of-plane motion due to lateral, in-plane motions should also be carefully considered in high-speed scanner designs. The coupling between in-plane and out-of-plane motions must be minimized since unwanted out-of-plane motions caused by in-plane motions lead to topographic errors. One obvious method to minimize out-of-plane motions is to increase the height and thickness of the flexures. However, a level of increase in the height and thickness of the flexures must be limited since taller and thicker flexures result in larger stiffness and, in return, reduced motional range of the scanner. We were also limited by the maximum allowable vertical travel range of the inverted microscope objective, which is about 10 mm. These two constraints put the limit of the proposed scanner's height at about 11 mm. The detailed CAD model of the proposed scanner is shown in Fig. 1.

3.2 Finite element analysis

From the modal analysis for the final scanner design, the resonant frequencies in the lateral scanning directions were predicted to occur at 7.75 and 7.95 kHz as shown in Figs. 2(d) and 2(e), respectively. Increasing the height of the flexures in the out-of-plane and therefore high stiffness in the *Z*-direction is one of the common ways of ensuring that the first resonant mode occurs in the lateral direction. Although the first three resonant modes were out-of-plane modes, the response of those motions shown in Figs. 2(a)–2(c) were very small as revealed in the AC response analysis compared to the first lateral resonant mode.

Also predicted was the maximum scan range achievable by the scanner, and this was found to be about 4.5 μm with the applied voltage of 100 V. As a reference, the maximum scan range of the original commercial scanner is 100 μm. This represents a reduction in the scan range by a factor of about 20. Since the bandwidth and the maximum scan range of a scanner are inversely dependent, achieving a higher bandwidth requires some level of scan range reduction.

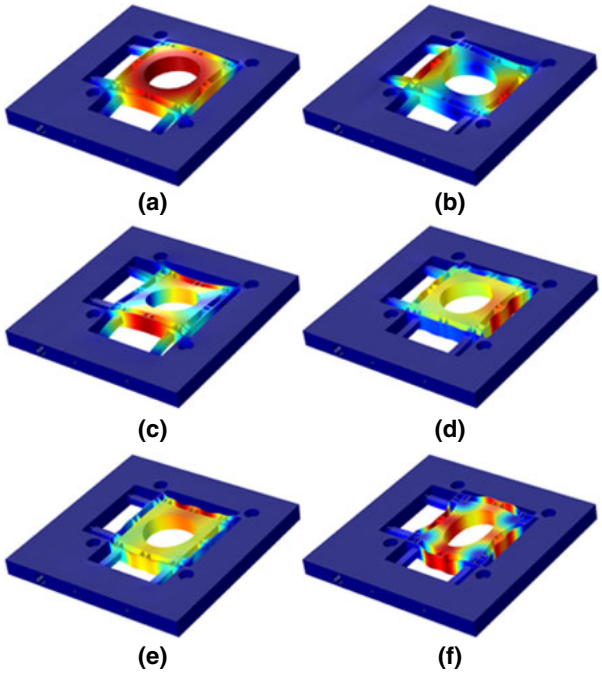

Fig. 2. (Color online) FEA results showing the first six modes of the proposed kinematic scanner predicted using COMSOL Multiphysics. The first three modes (a), (b), and (c) are out-of-plane modes occurring at 4.36, 5.95 and 6.98 kHz, respectively. The last three modes occurred along the lateral direction at frequencies of (d) 7.75, (e) 7.96, and (f) 10.00 kHz.

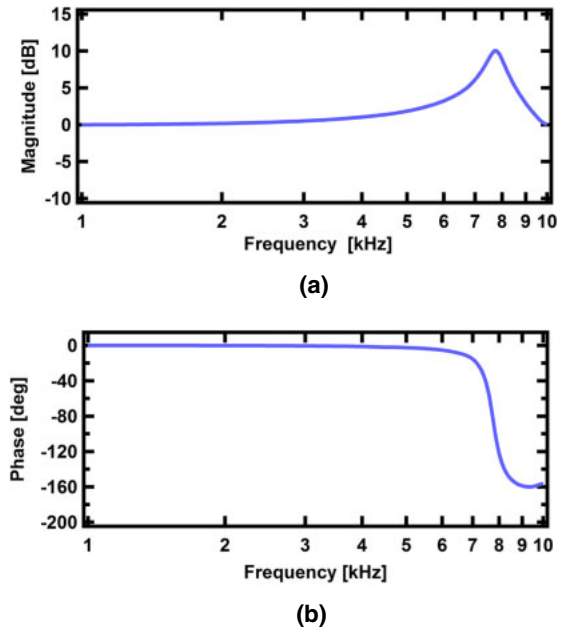

Fig. 3. (Color online) FEA results of the frequency sweep response of the custom scanner. The first resonant frequency occurred at about 7.8 kHz in both *X*- and *Y*-directions. Due to similarities in the data for both axes, only the *X*-axis result is presented.

Figure 3 shows both amplitude and phase vs frequency responses of the proposed scanner obtained from finite element analysis. In the simulation, the frequency of 1 V (peak-to-peak) sinusoidal excitation to the piezoelectric actuators was swept from 1 to 10 kHz and the corresponding response was calculated. The first significant resonant mode of the scanner occurred at about 7.8 kHz in both *X*- and *Y*-directions. As shown in Fig. 3, there are no visibly

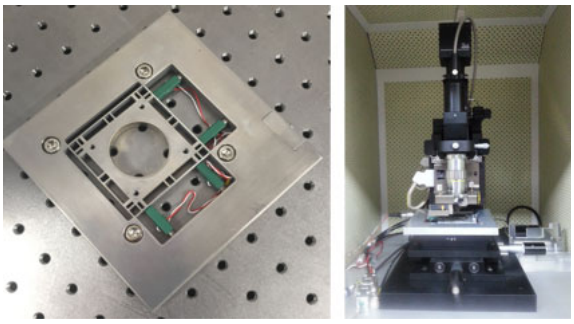

Fig. 4. (Color online) Fully assembled scanner (a) with four piezoelectric actuators installed in parallel configuration. The scanner has high stiffness in the vertical direction to suppress out-of-plane motions. (b) Picture of the modified commercial AFM.

significant effects from the first three out-of-plane modes of the flexure scanner.

3.3 Experimental *X*–*Y* scanner characterization

The fully assembled scanner with piezoelectric stacks installed is shown in Fig. 4(a). Also shown alongside is the commercial AFM (Park Systems XE-70) with its default *X*–*Y* scanner replaced with the new, high-speed scanner [Fig. 4(b)]. The new scanner has been fastened onto the coarse *X*–*Y* translation stage for a direct integration with no further hardware modification to the original AFM system.

For operation, each axis of the scanner is driven by a set of two piezoelectric stack actuators (NEC/TOKIN AE0505D16DF) with the drive voltage up to 100 V. A set of two piezoelectric actuators per axis are arranged in parallel to provide the thrust required to move the centrally located moving sample stage with an aperture, a feature necessary for an optical access from below. An appropriate level of driving power is required due to the mass of the moving stage and high stiffness of the flexures required for high-speed operation. The two parallel piezoelectric stacks are also strategically positioned away from the center to ensure that the moving stage with the central aperture does not deform significantly. Even a slight amount of deformation of the central aperture will act as a direct source of precision error in the positioning accuracy. Pre-loading of the actuator was effectively achieved by using fine-pitched screws (Thorlabs F3ES20) fitted to the frame.

The actual displacement vs drive voltage was measured by using a capacitive sensor (ADE Technologies 5810). The measured maximum scan range of the fabricated scanner was found to be 4.52 μm at 100 V, in close accordance with the predicted value of 4.5 μm from the finite element analysis.

The frequency response of the fabricated scanner was also measured using a dynamic signal analyzer (National Instruments PXI-4461). During the frequency response analysis, the scanner must operate in the linear regime in order to minimize any element of hysteresis.[38] Therefore, a sinusoidal excitation with an amplitude less than 1 V was applied to the piezoelectric actuators. In order to improve the signal to noise ratio, the average of 15 independent measurements were used for further analyses. The measured AC response of the scanner shows that the dominant resonance peaks occurred at 6.23 and 6.16 kHz in the *X*- and *Y*-direction, respectively. These measured values are slightly smaller than the

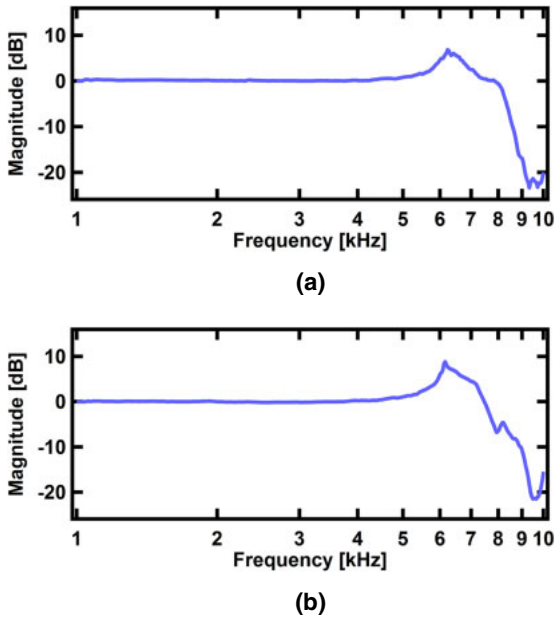

Fig. 5. (Color online) The measured frequency response of the developed high-speed piezoelectric scanner. (a) *X*-direction and (b) *Y*-direction.

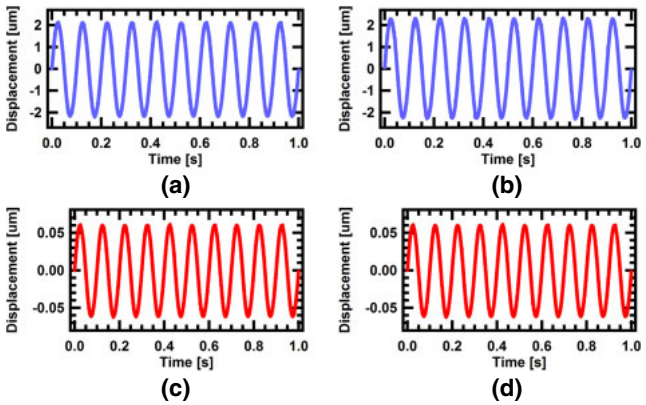

Fig. 6. (Color online) Measured displacements (a) *X*-direction and (b) *Y*-direction. Measured cross-coupling (c) *Y*-direction motion induced by movements in *X*-direction and (d) *X*-direction motion induced by movements in *Y*-direction.

simulation results, but this can be attributed to the inevitably non-uniform flexure thickness due to the non-ideal machining tolerances. The measured frequency responses (amplitude only) of the scanner in the *X*- and *Y*-directions are as shown in Fig. 5.

We also measured the cross-coupling of the proposed high-speed scanner by using a capacitive sensor positioned orthogonal to the actuation direction, and the induced displacements in the orthogonal directions were found to be 3.0 and 2.6% in the *X*- and *Y*-directions, respectively (see Fig. 6). It was, however, noted that pre-loading had a significant influence on the level of cross-coupling, and therefore it is necessary to minimize the effects of cross-coupling by properly adjusting the level of pre-loading.

Another very important parameter that negatively influences the performance of the scanner is hysteresis. Hysteresis of the high-speed scanner was measured in both *X*- and *Y*-axes, and the results are shown in Fig. 7. The root-mean-square errors (RMSE) due to hysteresis approximated using Eq. (1)

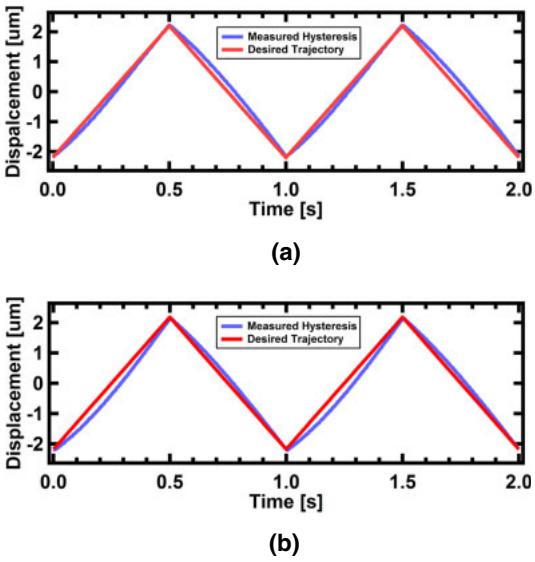

Fig. 7. (Color online) Measured hysteresis of the high-speed scanner (a) in *X*-axis and (b) in *Y*-axis.

Table I. The summary of measured characteristics of the fabricated parallel-kinematic high-speed scanner.

	X-axis	*Y*-axis
Scan range (μm)	4.52	4.57
Resonant frequency (kHz)	6.23	6.16
Cross-coupling (%)	3.00	2.60
Hysteresis, RMSE (%)	4.02	5.16
Hysteresis, e_{max} (%)	6.61	6.92

were found to be 4.02 and 5.16% in the *X*- and *Y*-directions, respectively, whereas the tracking error (e_{max}) (also called the percentage maximum absolute error, MAE) obtained using Eq. (2) was 6.61 and 6.92% in the *X*- and the *Y*-direction, respectively. A summary of the realized scanner characteristics are shown in Table I.

$$e_{max} = \text{MAE}\ (\%) = \frac{\max|\mathbf{y}-\mathbf{r}|}{\max\mathbf{y}-\min\mathbf{y}} \times 100\% \quad (1)$$

$$\text{RMSE}\ (\%) = \frac{\sqrt{\frac{1}{N}\sum_{i=1}^{N}(y_i - r_i)^2}}{\max\mathbf{y}-\min\mathbf{y}} \times 100\% \quad (2)$$

where $\mathbf{y} = [y_0, y_1, \ldots, y_{N-1}]$ and $\mathbf{r} = [r_0, r_1, \ldots, r_{N-1}]$.

3.4 Imaging results

In order to demonstrate the improvement in the scanning speed of a commercial AFM (Park Systems XE-70), a piece of a manufactured Blu-ray disk was used as a test sample. A Blu-ray test sample has relatively fine topographical features (pitch of about 300 nm) and can be easily prepared for imaging. Blue-ray data tracks were uncovered by using a pair of sharp tweezers to lift the upper protective layer. Then, the piece with exposed data tracks was secured on a glass slide for AFM imaging.

Non-contact mode imaging in air was used to obtain topographic images in the open-loop configuration for both commercial and custom-made scanners because the closed-loop control of the scanner limits the bandwidth of operation. The AFM was operated in ambient temperatures using

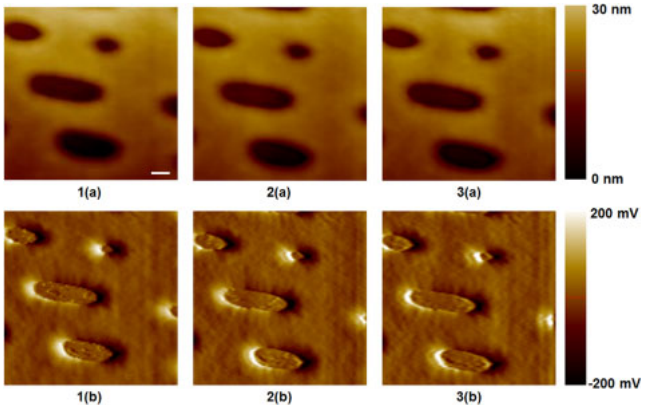

Fig. 8. (Color online) Typical images obtained by the unmodified XE-70 AFM at different scan rates, (a) topography and (b) error signal. The resolution was fixed at 128 × 128 pixels and the scan size was 2.2 × 2.2 μm^2. 1: 1 Hz; 2: 5 Hz; 3: 10 Hz. The quality of topographical images start to deteriorate beyond the line scan rate of 5 Hz. The scale bar is 300 nm.

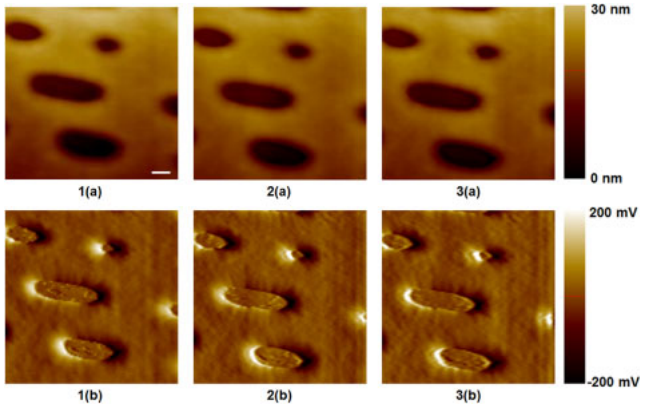

Fig. 9. (Color online) Typical images obtained by using a modified XE-70 AFM with the new high-speed *X*–*Y* scanner at different line scan rate. The resolution was fixed at 128 × 128 pixels with the scan size of 1.2 × 1.2 μm^2: (a) topography and (b) error signal, 1: 10 Hz, 2: 30 Hz, and 3: 50 Hz. The images show good tracking of the sample topography up to the scan rate of 50 Hz. The scale bar is 200 nm.

tapping mode cantilevers (Veeco Instruments TESP) with the nominal resonance frequency of about 300 kHz. The scan size of 2.2× by 2.2 μm^2 at the resolution of 128 × 128 pixels was chosen for imaging. When we performed the scans with the unmodified AFM (Park Systems XE-70), qualitative degradations in the topographical as well as the error signal images started to appear at the scan rate of 5 lines per second. Typical images obtained during the scans are shown in Fig. 8. The only post-image processing done was leveling to remove the linear slope in the images. The topographical images obtained shows vertical ripples that could be attributed to the vibrations in the fast axis of the scanner at elevated speeds.

Then, the same Blu-ray disk sample was scanned with the modified XE-70 AFM. Typical topographic and error-signal images obtained at different scan speeds are shown in Fig. 9. There were no noticeable oscillations or other artifacts observed in the images acquired at the scan speed of up to 50 Hz, clearly demonstrating the speed improvement from the unmodified XE-70 AFM (refer to Fig. 8). Beyond 50 Hz, the commercial AFM's *Z*-scanner could not provide fast enough feedback in the vertical (*Z*-) direction needed for tracking surface topography at high speeds.

It is noted that no other hardware or software change was made to the original commercial system other than replacing the default *X*–*Y* scanner. Additionally, our scanner has been intentionally designed with a large hole in the center. This particular design was a direct consequence of our intention to use the scanner on an inverted microscope in future experiments. Since samples would be accessible from the top and bottom of the scanner, simultaneous optical and AFM imaging would be possible. If this feature shall be abandoned, the central moving platform of the scanner can be made much smaller to yield even higher operating speeds.

4. Conclusions

We have successfully demonstrated a simple speed upgrade path for an aging commercial AFM system by incorporating a high-bandwidth scanner. This was possible by exploiting the fact that the slow *X*–*Y* scanner and not the AFM control electronics was the cause of the speed limitation. Therefore, the slow *X*–*Y* scanner of the commercial AFM system can be replaced with a custom-designed high-speed scanner to increase the operating speed while all other aspects of the system can remain unchanged. Our modified AFM system demonstrated a ten-fold increase in imaging speed. Although the maximum scan range has been decreased with the modified system, some experiments where speed is more important than the scan size can benefit from our approach to high-speed imaging. Since only the scanner has been replaced, an operator may change back to the original scanner at any time if a larger scan range is needed. Similar approach to improve scanning speed should be possible to other commercial AFM systems as well.

Acknowledgments

This research was supported by the Basic Science Research Program through the National Research Foundation of Korea (NRF) funded by the Ministry of Education (2015R1D1A1A01059003) and the National Research Foundation of Korea (NRF) grant funded by the Korean government (MSIP) (2015R1C1A2A01052717 to S. Park).

1) K. Iwata, S. Yamazaki, P. Mutombo, P. Hapala, M. Ondracek, P. Jelinek, Y. Sugimoto, K. Park, J. Lee, Z. Zhang, and W. King, Nat. Commun. **6**, 7766 (2015).
2) A. L. Pyne and B. W. Hoogenboom, Methods Mol. Biol. **1431**, 47 (2016).
3) M. Shibata, H. Watanabe, T. Uchihashi, T. Ando, and R. Yasuda, Biophys. Physicobiol. **14**, 127 (2017).
4) L. Almonte and J. Colchero, Nanoscale **9**, 2903 (2017).
5) J. Ren and Q. Zou, Beilstein J. Nanotechnol. **8**, 1563 (2017).
6) D. Alsteens, D. J. Muller, and Y. F. Dufrene, Acc. Chem. Res. **50**, 924 (2017).
7) J. Zhong and J. Yan, RSC Adv. **6**, 1103 (2016).
8) A. Shiotari and Y. Sugimoto, Nat. Commun. **8**, 14313 (2017).
9) P. Schön, Methods **103**, 25 (2016).
10) S. Guo, X. Zhu, D. Jaczewski, S. S. Lee, T. He, S. L. Teo, and G. J. Vancso, Nat. Nanotechnol. **11**, 817 (2016).
11) D. V. Korneev, A. V. Popova, V. M. Generalov, and B. N. Zaitsev, Cell Biophys. **61**, 413 (2016).
12) Y. K. Kim, W. Kim, and J. W. Park, Bull. Korean Chem. Soc. **37**, 1895 (2016).
13) B. H. Kim, N. Y. Palermo, S. Lovas, T. Zaikova, J. F. W. Keana, and Y. L. Lyubchenko, Biochemistry **50**, 5154 (2011).
14) Q. Tang, S. Q. Shin, and L. Zhou, J. Nanosci. Nanotechnol. **4**, 948 (2004).

15) J. Deng, J. Dong, and P. Cohen, Procedia Manuf. **5**, 1283 (2016).
16) T. Hugel and M. Seitz, Macromol. Rapid Commun. **22**, 989 (2001).
17) O. D. Payton, L. Picco, and T. B. Scott, Int. Mater. Rev. **61**, 473 (2016).
18) M. Marrese, V. Guarino, and L. Ambrosio, J. Funct. Biomater. **8**, 7 (2017).
19) M. Li, L. Liu, N. Xi, and Y. Wang, IEEE Nanotechnol. Mag. **9**, 25 (2015).
20) S. Darwich, K. Mougin, A. Rao, E. Gnecco, S. Jayaraman, and H. Haidara, Beilstein J. Nanotechnol. **2**, 85 (2011).
21) A. H. Korayem, M. H. Korayem, and M. Taheri, Arab. J. Sci. Eng. **40**, 2685 (2015).
22) V. Bouchiat and D. Esteve, Appl. Phys. Lett. **69**, 3098 (1996).
23) K. Miyake, N. Satomi, and S. Sasaki, Appl. Phys. Lett. **89**, 031925 (2006).
24) J. Kreith, T. Strunz, E. J. Fantner, G. E. Fantner, and M. J. Cordill, Rev. Sci. Instrum. **88**, 053704 (2017).
25) M. Marchetti, G. J. L. Wuite, and W. H. Roos, Curr. Opin. Virol. **18**, 82 (2016).
26) Y. Ding, G. K. Xu, and G. F. Wang, Sci. Rep. **7**, 45575 (2017).
27) L. M. Demers, D. S. Ginger, S. Park, Z. Li, S. Chung, and C. A. Mirkin, Science **296**, 1836 (2002).
28) S. Hasegawa, S. Yamada, T. Yamada, J. Shirakashi, and Y. Takemura, IEEJ Trans. Electr. Electron. Eng. **3**, 382 (2008).
29) S. Masubuchi, M. Arai, and T. Machida, Nano Lett. **11**, 4542 (2011).
30) J. Shirakashi, M. Ishii, K. Matsumoto, N. Miura, and M. Konagai, Jpn. J. Appl. Phys. **35**, L1524 (1996).
31) G. J. Yong, W. E. Vanderlinde, E. K. Tanyi, D. M. Schaefer, C. Stumpf, and R. M. Kolagani, J. Vac. Sci. Technol. B **34**, 021601 (2016).
32) A. J. Fleming, IEEE Trans. Contr. Syst. Technol. **19**, 156 (2011).
33) J. D. Adams, A. Nievergelt, B. W. Erickson, C. Yang, M. Dukic, and G. E. Fantner, Rev. Sci. Instrum. **85**, 093702 (2014).
34) G. Schitter and A. Stemmer, IEEE Trans. Contr. Syst. Technol. **12**, 449 (2004).
35) A. P. Nievergelt, W. E. Blake, H. Nahid, D. A. Jonathan, and E. F. Georg, Sci. Rep. **5**, 11987 (2015).
36) Y. K. Yong, S. O. R. Moheimani, B. J. Kenton, and K. K. Leang, Rev. Sci. Instrum. **83**, 121101 (2012).
37) G. Schitter, K. Astrom, B. DeMartini, P. Thurner, K. Turner, and P. Hansma, IEEE Trans. Contr. Syst. Technol. **15**, 906 (2007).
38) K. K. Leang, Q. Zou, and S. Devasia, IEEE Contr. Syst. Mag. **29**, 70 (2009).